Accepted Manuscript
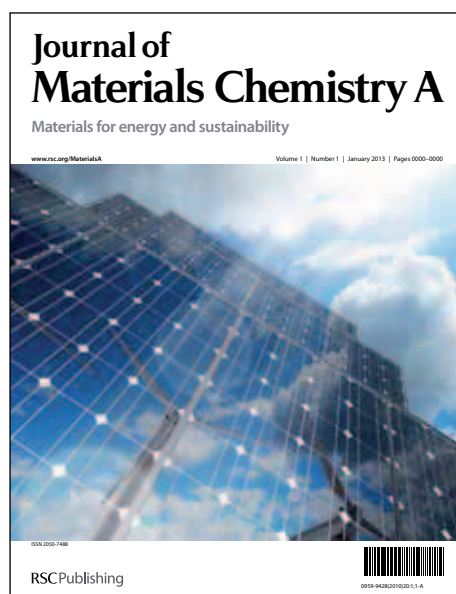
This is an *Accepted Manuscript*, which has been through the RSC Publishing peer review process and has been accepted for publication.

Accepted Manuscripts are published online shortly after acceptance, which is prior to technical editing, formatting and proof reading. This free service from RSC Publishing allows authors to make their results available to the community, in citable form, before publication of the edited article. This *Accepted Manuscript* will be replaced by the edited and formatted *Advance Article* as soon as this is available.

To cite this manuscript please use its permanent Digital Object Identifier (DOI®), which is identical for all formats of publication.

More information about *Accepted Manuscripts* can be found in the **Information for Authors**.

Please note that technical editing may introduce minor changes to the text and/or graphics contained in the manuscript submitted by the author(s) which may alter content, and that the standard **Terms & Conditions** and the **ethical guidelines** that apply to the journal are still applicable. In no event shall the RSC be held responsible for any errors or omissions in these *Accepted Manuscript* manuscripts or any consequences arising from the use of any information contained in them.

Journal Name

Journal of Materials Chemistry A

ARTICLE TYPE

From core-shell MoS$_x$/ZnS to open fullerene-like MoS$_2$ nanoparticles.

Elodie Blanco, Denis Uzio, Gilles Berhault, Pavel Afanasiev*[a],

₅ A new two-step solution route has been developed for the preparation of hollow inorganic fullerene-like (IF) MoS$_2$ particles with quantitative yield. First, core-shell MoS$_x$/ZnS (x~3-4) particles were synthesized by depositing amorphous MoS$_x$ on the ZnS seeds in a solution containing ethylene glycol and elemental sulfur. Core-shell particles contain 7-9 nm size ZnS core surrounded with amorphous MoS$_x$ sulfide shell. Then the core–shell particles were thermally treated at 400-750 °C. As a result, 20-50 nm size IF-like ₁₀ MoS$_2$ was crystallized, whereas ZnS left the particles interior and formed bulky crystals aside. At the moment of ZnS crystallization a burst-out of the MoS$_2$ walls occurs and the resulting IF particles contain openings, which make the internal voids acessible for gas adsorption. By means of varying the Mo/Zn ratio in the solvothermal reaction mixture, the number of slabs in the onion–like particles can be controlled. Due to the intermediate presence of the ZnS core, relatively large voids are created in the ₁₅ resulting IF-MoS$_2$. The solids as obtained possess high specific surface area, enhanced thiophene HDS activity and exceptional thermal stability. Particles size and wall thickness can be controlled by means of variation of the Mo/Zn atomic ratio in the solution.

1. Introduction

The design of materials morphology represents one of the ₂₀ greatest technological and scientific challenges.[1] Nanodispersed sulfides of group VI transition metals are important class of inorganic materials for heterogeneous catalysts,[2,3] electrocatalysts[4] photocatalysts,[5] lubricants,[6] anodes for Li-ion batteries,[7,8] photoluminiscent materials,[9] polymer ₂₅ nanocomposites[10] and many other applicatins. Since the inorganic fullerenes (IF) of metals sulfides MX$_2$ (M=Mo, W; X= S, Se) have been discovered by Tenne and co-workers,[11] a large variety of forms including nanoparticles, nanotubes, nanosheets, nanofibers, and nanobelts have been obtained.[12,13] Meanwhile, ₃₀ developing a simple and effective method for large-scale chemical synthesis of high quality IF-MoS$_2$ still remains a challenge. The existing approaches provide energy consuming and hardly scalable procedures with moderate yields of the desired IF particles.

₃₅ Molybdenum sulfide constitutes the main active component of the existing hydrotreating catalysts.[14] The new class of highly loaded or unsupported sulfide catalysts contain MoS$_2$ promoted with cobalt or nickel, mixed with some small amounts of binders and/or textural promoters. To produce molybdenum sulfide with ₄₀ controlled morphology, several techniques have been developed, such as arc discharge[15], chemical vapor deposition[16] hydrothermal,[17] solvothermal,[18] sonochemical[19] and biotemplate[20] syntheses. Recently we demonstrated that the catalysts containing IF-MoS$_2$ show original properties due to the ₄₅ abundance of curved planes.[21]. To prepare IF-MoS$_2$ we used a

solution method in which thiodimolybdate precursor was refluxed in acetone[22]. Only small yields of IF-MoS$_2$ were available, with no control of the particles size.

₅₀ Several attempts were undertaken to prepare fullerene-like molybdenum sulfide by solution ways. These solution techniques all include preliminary formation of an amorphous precursor, which can be obtained from thiomolybdate precipitation with an acid,[23] microwave heating,[24] sonochemical reaction[25] or hydrothermal reaction.[26] Preparation of amorphous precursor is ₅₅ followed by thermal annealing, leading to crystallization of MoS$_2$. If curved fullerene-like objects are indeed present in such preparations, obtaining of pure IF-MoS$_2$ with narrow size distribution remains difficult. The critical point is preparing of loosely agglomerated precursor particles with uniform shape and ₆₀ size.

Seed-induced precipitations are well adopted to the preparation of narrow particle size distributions, because of better control of nucleation. Being widely studied for the core shell semiconducting sulfides such as zinc and cadmium sulfides and ₆₅ selenides,[27,28] to our knowledge the seed-assisted solution reactions have never been used to prepare molybdenum sulfide.

Here we report on a new seed-assisted solution route to the IF-MoS$_2$ allowing large–scale synthesis with quantitative yield and possibility to control the particles size. The proposed preparation ₇₀ technique is extremely simple and uses the least onerous precursors which are ammonium heptamolybdate and elemental sulfur combined to ZnS used as a seed.

Experimental

Preparation techniques.

All chemicals were high purity grade purchased from Aldrich. To prepare ZnS seeds, to 100 ml of 0.1 M solution of $Zn(NO_3)_2$ or $ZnCl_2$ were added 50 ml of 0.1 M nonahydrated sodium sulfide. White precipitate was separated by centrifugation, washed with ethanol and again centrifuged. Then 200 ml of EG were added and the mixture was dispersed by ultrasound for 2 h and kept in oven at 80 °C for 24h. Stable colloidal suspension of ZnS seed was obtained.

In a typical core-shell particles synthesis, to 100 ml of ethylene glycol (EG) were added 3.2g of elemental sulfur. The mixture was placed in a vessel with reverse refrigerator, heated under stirring to the boiling temperature of ethylene glycol (196 °C) and refluxed at this temperature for 1 h. Then two solutions both pre-heated to 180°C were added rapidly, one after another: 1.75 g ammonium heptamolybdate in 50 ml EG and an appropriate amount of ZnS suspension in EG. In the preparations with variable Zn/Mo ratio, the amount of molybdenum was fixed, that of Zn varied.

The solutions were rapidly mixed upon vigorous stirring and the temperature was raised to the boiling point of EG (198°C). The reaction mixture was refluxed for 1h and then cooled to room temperature. Brown powder product was separated by centrifugation and washed with warm acetone to remove unreacted sulfur. The product was ovendried and kept under inert atmosphere.

Thermal treatment was carried out in a quartz reactor in the range of temperatures 400 -750°C. Approximately 0.5 g of precursor was heated for 2 h under a flow of 3.6 l/h of a gas (N_2, H_2) or a gas mixture (H_2S/H_2, H_2S/N_2). Heating rate was 5 °C /min.

Characterizations and catalytic tests.

Temperature-programmed reduction (TPR) was carried out in a quartz reactor. Samples of sulfides (ca. 0.005–0.01 g) were heated under a hydrogen flow (50 cm^3/min) from room temperature to 1050 °C at a rate of 5° min^{-1}. The H_2S evolved in the reduction was detected by means of an HNU photoionization detector equipped with a 10.2 eV UV light source. Simultaneously, the evolving gases were detected by a VG Thermo quadrupole mass-spectrometer. The amount of H_2S released from the solid was quantified after calibration of the detector with a gas mixture of known H_2S content.

Transmission electron microscopy (TEM) was carried out on a JEOL 2010 device with an accelerating voltage 200 keV. The samples were dispersed in n-hexane by ultrasound, and then put onto a holey carbon filament on a copper grid sample holder. In order to protect them from oxidation by air, the samples still covered with liquid hexane were immediately introduced into the TEM vacuum chamber. The analysis of images (slabs stacking and length) was carried out using Digital Microgtaph Gatan™ software. The average slab lengths (L) and stacking layer numbers (N) were calculated as the first moments of the respective distributions.

Nitrogen adsorption-desorption isotherms were measured on a Micromeritics ASAP 2010 instrument. Specific surface area was calculated using BET equation and pore size distributions in the mesopores domain were calculated by the Barrett–Joyner–Hallenda (BJH) method. Prior to measurements the samples were heated in a secondary vacuum at 300 °C for 4h. The X-ray diffraction (XRD) patterns were obtained on a Bruker diffractometer with Cu-Kα emission and identified using standard JCPDS files. Mean particles size was determined using the Scherrer equation. The metals content in the synthesized solids was determined, after dissolution in a HNO_3/H_2SO_4 mixture, by plasma-coupled atomic emission spectroscopy (AES-ICP). The sulfur and carbon contents were measured with a Strohlein Instruments CS-MAT 5500 analyzer.

Catalytic activities were measured for thiophene hydrodesulfurization (HDS) at atmospheric pressure in a fixed-bed flow microreactor. In the chosen temperature range, 280–340 °C, the thiophene conversion at the partial pressure P(thiophene)=2.7 kPa was below 10% under the conditions used (50 ml/min gas flow, 70–200 mg of catalyst), and the plug-flow reactor model was used to calculate the specific reaction rate, Vs, according to equation.

$$Vs = - (F/m)ln(1-x)$$

where F is the thiophene molar flow (mol/s), m is the total solid catalyst mass (g), and x is the thiophene conversion. Catalytic activity of different samples was compared after attaining stable conversion of thiophene, occurring after ca. 16 h of on-stream reaction.

Results and discussion

Preparation and properties of the solids.

The general approach is to use a polar solvent with a relatively high boiling point (ethylene glycol, EG) and elemental sulfur. Previously we reported on the use of a similar reaction mixture to prepare biotemplated MoS_2, replicating cellulose morphology.[29, 30] Elemental sulfur is cheap and non-toxic, making the procedure environmentally friendly. A highly boiling solvent allows carrying out the solution reaction at atmospheric pressure, since the temperature can be raised high enough to achieve significant reactivity of dissolved sulfur. Otherwise, if water or another low-boiling solvent is applied as the reaction medium, hydrothermal equipment is necessary. The reaction in the solution occurs as an exchange between the dissolved molybdate and sulfur to produce intermediate thiomolybdate molecular species that further condense leading to the amorphous sulfide MoS_x (3<x<4) with intermeriate oxidation of molybdenum between 4 and 5. In the absence of a seed or a template, the reaction occurs homogeneously via intermittent formation of dark–red transparent solution. The solid product collected after 4 h consists of highly agglomerated particles of circa 300-500 nm size (Fig. S1 of Supporting Information). To decrease the size of the particles the nucleation step should be accelerated by means of a seed.
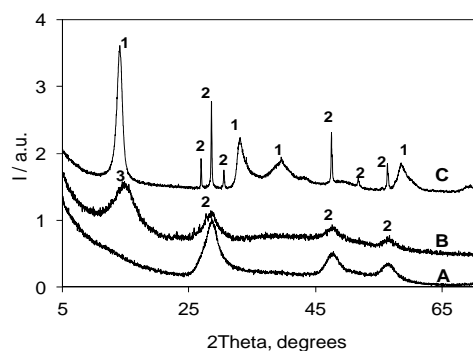
Fig. 1. XRD patterns of ZnS seed (A), the solid after solution reaction (B)
and the same solid treated at 750 °C under H_2S/H_2 flow (C). Peaks marks:
1 – MoS_2; 2 – ZnS; 3 - MoS_{3+x}.

In this work we applied as a seed nanodispersion of zinc
sulfide in EG. ZnS was prepared according to the literature by
means of precipitation of $Zn(NO_3)_2$ or $ZnCl_2$ aqueous solutions
with sodium sulfide.[31] White precipitate, immediately formed
after mixing of the corresponding solutions, was separated by
centrifugation and then re-dispersed in EG by ultrasonication.
Colloidal suspension of ZnS in EG is stable for indefinite time.
As shown by transmission electron microscopy (TEM), ZnS
material has the primary particle size near 7 nm if prepared from
the $Zn(NO_3)_2$ precursor and ca 9 nm when using $ZnCl_2$ (Fig. S2).
Powder X-ray diffraction (XRD) attests that the particles of ZnS
are poorly crystalline (Fig. 1a). BET surface areas measured for
the samples prepared from $Zn(NO_3)_2$ and $ZnCl_2$ are 197 and 155
m^2/g nm, respectively. Particle size determined from the XRD
line broadening according to Scherrer equation agrees well with
the size determined from TEM and BET surface measurements.
The ZnS colloidal suspension was further applied as a seed for
the solution reaction of ammonium heptamolybdate and sulfur in
EG. After the reaction dark brown precipitate was obtained. In
this solid, beside the initial ZnS, XRD showed a new broad
maximum, corresponding to non-stoichiometric MoS_x (3<x<4).
At the same time TEM revealed formation of weakly
agglomerated spherical particles of 20-70 nm size (Fig. 2a).

Elemental analysis of the solids prepared with solution ratios
Mo/Zn=1 and Mo/Zn=2 revealed respectively the stoichiometric
formula $Zn_{0.97}MoS_{4.8}$ and $Zn_{0.44}MoS_{3.9}$. Such compositions
correspond to the mixtures of ZnS with non-stoichiometric
amorphous molybdenum sulfide MoS_x. Since the Zn to Mo
atomic ratios in the solid products were close to those loaded in
the solutions, complete reaction of molybdenum species is
achieved. However, Mo/Zn ratio observed by the TEM EDX
analysis was systematically higher than its elemental analysis
value, i.e. the samples are seemingly deficient in Zn (Table S1).
As the characteristic depth of the TEM EDX analysis correlates
with the transparency of the samples observed in the TEM
images, for the non-transparent agglomerates of nanoballs of
several tens nm size, zinc sulfide should be hidden from the EDS
observation, being screened by the amorphous MoS_x. Therefore
the ZnS grains stay mostly inside the composite particles, which

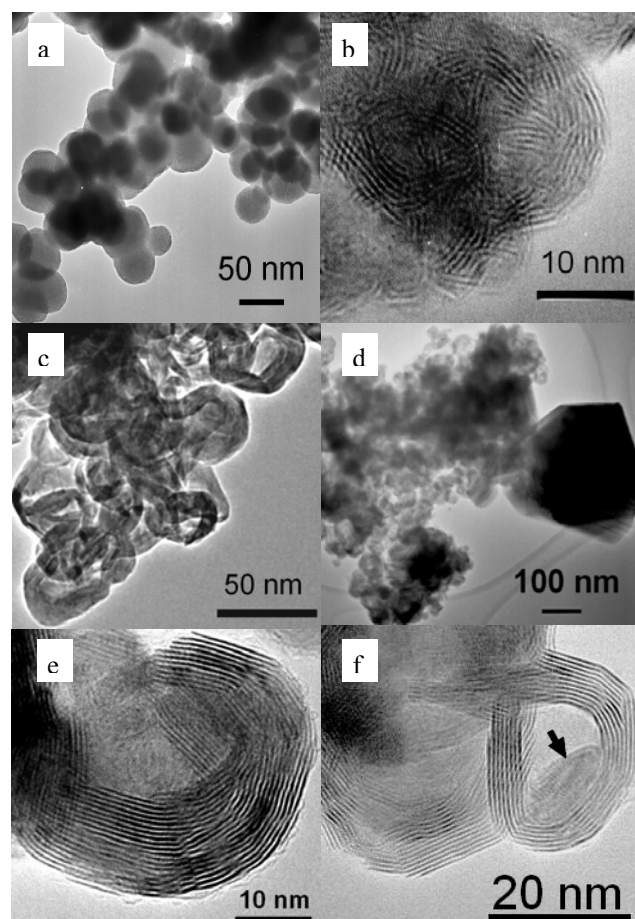can be expected as they probably initiate the onset of MoS_x
nucleation.

Fig. 2. TEM images of the amorphous solid after solution reaction (a);
disordered MoS2 fringes formed at 400 °C (b); agglomerate of hollow IF-
like particles after treatment at 750 °C (c); agglomerate of IF-like MoS_2
particles and a large crystallite of ZnS (d); hollow IF-like particle with an
opening (e) and rarely observed IF particle containing a piece of trapped
ZnS (indicated by an arrow) (f).

TEM study reveals substantial difference of the particle size as a
function of the Mo/Zn ratio. Preparations with Mo/Zn=1 have
smaller particles size (15-60 nm, mean size 36 nm, Figure S3a)
than prepared with Mo/Zn=2 (30-80 nm, mean size 60 nm; Figure
S3b). This effect naturally follows from the greater number of the
nucleation centres for Mo/Zn=1. No significant difference of the
particle size was observed for the materials grown on the ZnS
seeds prepared from $ZnCl_2$ or from $Zn(NO_3)_2$ precursors.
Thermal treatment of the core-shell particles under various gases
including H_2, N_2, H_2S/H_2 or H_2S/N_2 invariably leads to the
decomposition of MoS_x and crystallization of the MoS_2 slabs.
Depending on the nature of gas flow, the excess sulfur is released
either as H_2S or as elemental S_8 (the last forms yellow condensate
on the reactor walls). Decomposition of MoS_{3+x} to MoS_2 begins
at ca 250 °C and can be considered complete above 400 °C. The
decomposition was followed by *in situ* XRD under nitrogen flow
at progressively increasing temperature, with a step 50 °C (Figure
3). The peak of (002) reflection of MoS_2 phase appears at 300 °C
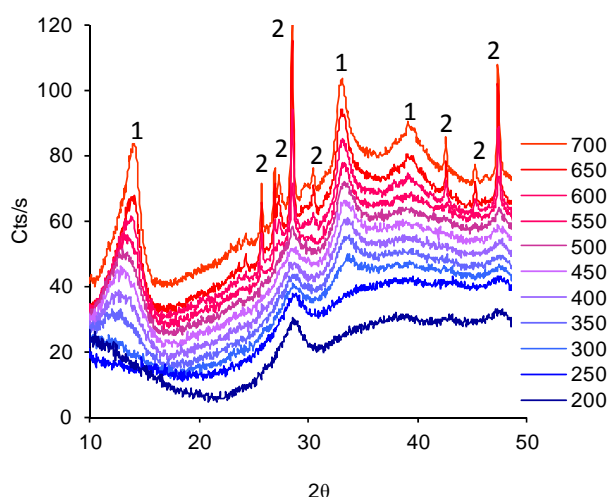and becomes intense at 350°. Further increase of temperature

Fig. 3 Thermal evolution of MoSx/ZnS followed by *in situ* XRD upon heating the core-shell solid with atominc ratio Mo/Zn=1 under nitrogen flow. Temperatures in °C are indicated at the right of the figure. Phases marks: 1- MoS_2; 2 – ZnS.

[5] leads to the gradual increase of the intensity of MoS_2 lines, suggesting progressive increase of the MoS_2 slabs length and stacking (Fig. S4). The (002) interplane distance corresponding to the separation between the slabs, decreases upon heating from ca 6.6 Å at 400 °C to 6.3 Å at 700°C. Such evolution corresponds to [10] progressive healing of the defects of the slabs packing and formation of more regular MoS_2 stacks. The (002) distance however never attained the literature value for bulk molybdenite (6.14 Å). Such shift of the (002) peak of the IF sulfides was previously observed and attributed to the strain in the bent [15] layers.[32]
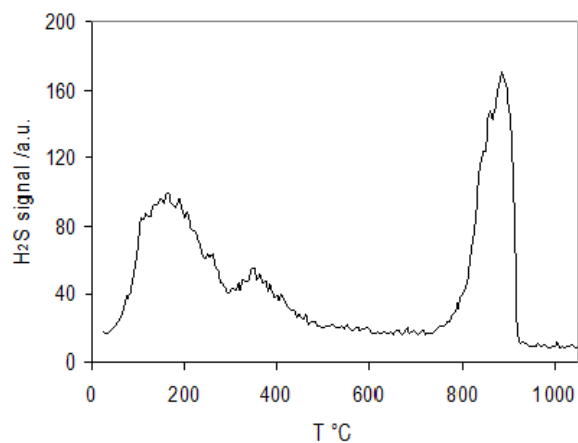

Fig. 4. Temperature programmed reduction under H_2 of the core-shell solid with atomic ratio Mo/Zn=1.

[20] Simultaneously with MoS_2 crystallization, but following quite a different trend, the evolution of the ZnS phase proceeded. Unlike MoS_2 which mostly crystallized between 300 and 400 °C, ZnS remained almost unchanged in this temperature region. Then,

after 500 °C a burst out of rapid formation of bulk-like ZnS was [25] observed. The particles size of ZnS as determined by Scherrer formula (350 nm) was significantly larger than that of the initial ZnS/MoSx core-shell solid. Therefore we can conclude on the basis of XRD data that ZnS leaves the initial particles and forms much larger crystals aside.

[30] Similar evolution was observed upon heating of core-shell particles in various gas flows, including pure H_2, always leading to the formation of IFs. Therefore temperature programmed reduction (TPR) in hydrogen is relevant and provides valuable information of the processes occurring upon formation of IF [35] solids. TPR of the initial core-shell solids under H_2 flow clearly shows a low-temperature peak corresponding to the transformation of S_2^{2-} species of amorphous MoSx into the S^{2-} of MoS_2 (Fig. 4), as discussed earlier.[33]

Comparing the TPR data with the results of *in-situ* XRD, we see [40] that in the temperature range below 300 °C H_2S is abundantly released without formation of crystalline MoS_2. Apparently considerable amount of sulfur can be removed from the non-stoichiometric MoS_{3+x} while it remains amorphous. Then after the maximum of sulfur release, (002) XRD line appeared due to [45] formation of MoS_2 stacks. Then above 400 °C, when the formation of the MoS_2 phase was completed, the amount of the released H_2S rapidly decreased. At higher temperatures no significant amounts of H_2S were released, even though the crystallization of MoS_2 continued according to XRD. No other [50] gases were formed during TPR in the range between 500 and 700 °C as monitored by a mass spectrometer in the m/z range from 2 to 100. Note also that the MoS_2 crystallization curve has a breakpoint near 450°C (Fig. S5), occurring at the same moment when the H_2S production drops down. Finally, above 700°C [55] progressive reduction of bulk MoS_2 to metallic molybdenum slowly begins. ZnS is not reduced in the whole range of temperatures, since the reduction thermodynamics is much less favourable than for MoS_2.

The results of *in situ* XRD and TPR studies provide a coherent [60] picture of the material evolution upon progressive heating from room temperature to 700 °C. Below 300 °C the MoS_{3+x} phase progressively decomposes whereas ZnS seed particles do not change. Then, between 300° and 450°C rapid crystallization of MoS_2 occurs, but ZnS particles still remain virtually unchanged. [65] Above 450° and up to 700 °C, MoS_2 crystallization becomes slower, while a burst out of formation of ZnS bulky crystals occurs.

Transmission electron microscopy (TEM) provides an additional insight into the evolution of the particles structure at different [70] stages of the thermal treatment. Whatever the treating gas, disordered short slabs of MoS_2 are formed at 400 °C (Fig. 2b). Further evolution at higher temperatures occurs with the increase of the slabs length and progressive formation of the onion -like concentric shell structure. IF-like particles are obtained in the [75] range of temperatures 600-750°C (Fig. 2c-f). Statistical analysis of TEM particle size shows that some shrinkage of MoS_x nanoballs occurred at 400°C, probably due to the release of excess sulfur (Fig. S3). Further heating leads only to a slight additional decrease of size (Table S1).

[80] Simultaneously with the formation of the IF structures, ZnS leaves the particles interior and forms large crystallites of

wurtzite (Fig 2d and Fig. 1c). EDS analysis attests virtually total separation of Zn and Mo sulfides at 700 °C (99.2 at.% Zn, 0.8 at.% Zn in the bulk crystal depicted in the figure). Thus, Mo/Zn ratio in the molybdenum-enriched zones represented in Fig. 2c, e is over 100. At the same time large crystallite in Fig. 2e contains only Zn and S in 1:1 molar ratio and no molybdenum at all. Since diffusion of Zn through the closed MoS_2 shells looks highly unlikely to occur, some openings should exist in the IF-like particles in order to provide the departure pathway for ZnS at high temperatures. Outward migration of ZnS hinders formation of totally closed shells. The materials obtained possess therefore a particular property of combining IF-like morphology with considerable amount of accessible voids. In many TEM images the openings in the IF particles are directly seen (Fig. 2e). In rare cases, however, small amounts of ZnS trapped inside the voids of closed IF particles could be found (Fig. 2f).
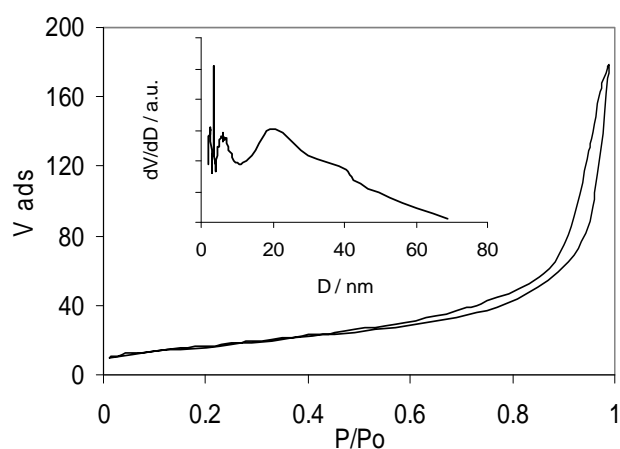

Fig. 5. Nitrogen adsorption – desorption isotherm for the solid obtained from the treatment at 750 °C in H_2/H_2S mixture. Inset: pore volume differential distribution.

Due to formation of open hollow particles, the specific surface areas (S_{sp}) of the solids evolve in an unusual manner upon the increase of the treatment temperature. Instead of dropping down as should occur for normal sintering, S_{sp} increases above 600°C, from ca 30 to more than 50 m^2/g, probably due to liberation of the particles voids (Table S1). S_{sp} of the solids treated at 750°C is almost twice higher than that of the same materials heated only to 400 °C. For this type of materials the solids obtained in this work show exceptionally high specific surface area and thermal stability. Thus, for the standard technique of MoS_2 preparation by decomposition of ammonium thiomolybdate, the value of S_{sp} drops from 50-60 m^2/g at 400°C to 3-5 m^2/g above 700° C. Nitrogen adsorption-desorption isotherms confirm the presence of open IF particles and reveal a specific feature due to the inner voids. All the samples show multimodal pore size distribution, consisting of the contributions of slabs packing defects and of the interparticle voids. However, a particular feature is observed for the solids treated at high temperature. A distinct maximum of pore size distribution appears at 15-20 nm (Fig. 5). Obviously, the voids inside the particles as seen in TEM are responsible for

this peak in the differential pore volume distribution. Remarkably, this feature is absent in the pore size distribution of the materials treated at 400°C (Fig. S6).
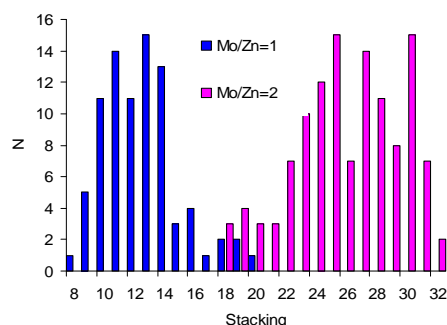

Fig. 6. Histograms of MoS_2 slabs stacking for two different Mo/Zn ratios. Both solids are treated at 750 °C in H_2S/H_2 flow

The size of the particles and the thickness of the IF walls can be controlled by varying Zn/Mo ratio in the reaction mixtures. The solids with Mo/Zn=1 consist of smaller particles with 11-15 layers, whereas for the Mo/Zn=2 the particles are larger and the layers stacking is between 20 and 30 (Fig. 6).
Expectedly, with the increase of ZnS amount in the precursor, hollow particles with thinner walls are obtained. However, the relative amount of zinc cannot be increased over a certain limit without losing the IF structure. Thus, for the Mo/Zn=0.33 no IF particles were obtained but just a dispersion of ZnS grains partially covered with discontinuous MoS_2 slabs. Upper limit of the Mo/Zn ratio corresponds to the situation where large particles of MoS_x solid begin to appear, of the same size as if no seed were present (300-500 nm). Such regime is certainly realized at the atomic ratio Mo/Zn = 20, when the morphology of the solid was indistinguishable from that grown without seed. However more precise value of the borderline Mo/Zr ratio is yet to be determined.
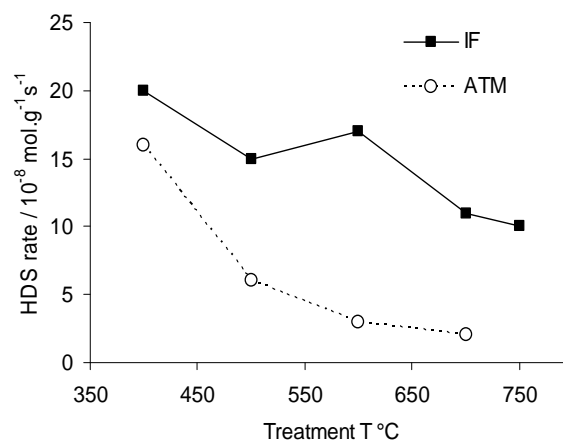

Fig. 7. Steady state thiophene HDS specific rate at 300 °C as a function of pre-treatment temperature for the IF catalysts (IF) and ATM decomposition products (ATM).

Thiophene hydrodesulfurization (HDS) test can be used as a simple benchmark reaction to evaluate the potentiality of the new

materials as catalysts. In Figure 7 are presented steady state levels of the HDS specific rate as a function of treatment temperature. The IF solids are compared to the reference bulk MoS_2, prepared by decomposition of ammonium thiomolybdate (ATM).
5 Thiophene HDS activation energy was in the range 75-85 kJ/mol, with no statistically significant differences between the solids and in agreement with previous studies.[34, 35] The specific HDS rate for the IF solids somewhat decreased with the treatment temperature. The HDS catalytic centers are believed to be located
10 at the edges and defects of the MoS_2 slabs.[2] Therefore, formation of longer slabs at increased temperatures implies a decrease of the density of catalytic centers. However, the drop of activity was by far lesser for the IF solids than for the reference ATM catalyst. Moreover, for the IF catalysts prepared at 600 °C, an increase of
15 activity was reliably observed. It is likely related to the liberation of the interior of the IF particles. As compared to the reference MoS_2, IF solids possess high surface area and great amount of curved or broken slabs. The slabs curvature contributes to preservation of the HDS activity as discussed in our recent
20 work.[21] As a result, exceptionally high thermal stability of the IF catalysts was observed.

The mechanism of the IFs formation necessarily includes the release of matter from the interior of the particles and perhaps has some common features with the "giant bubble shrinking"
25 mechanism as proposed by Tremel and coll.[36] At moderate temperatures (400-500 °C in our case) MoS_2 crystallizes and starts to form extended layers on the surface of the reacting particles. However at increased temperature crystallizing ZnS disrupts the MoS_2 shell in order to be liberated. We suppose that
30 the disruption occurs because crystallization of ZnS in the interior of the particles leads to the formation of anisotropic non-spherical crystallites with the dimension larger than the MoS_2 shells.

After the release of ZnS, empty MoS_2 shells slightly shrink to form dense IF particles. There are however two important points
35 of difference between the "giant bubble" mechanism and our observations. First, the burst–out and breaking the walls by crystallizing ZnS occurs at higher temperature (600-700 °C), when multi-layer IF-like shell of MoS_2 is already formed. Moreover no significant amount of gases was released between
40 500 and 700°C, as attested by mass spectrometry. In the TEM micrographs we do not see any significant dilatation of the particles to bubbles. Probably, since in our case the IF –MoS_2 particles are already well formed and rather rigid at the moment of the burst-out. By this reason they mostly remain opened, as
45 attested by the specific surface area measurements.

Conclusions

In summary, we developed a novel route to the IF-MoS_2 nanoparticles that allows large scale preparations with the
50 quantitative yield and the possibility of size tuning. The amount of materials available from such preparations is limited only by the volumes of the reactors used for the solution reaction and for the subsequent thermal treatment. Though we only briefly descried their catalytic properties, the materials described here
55 have multiple potential applications. They are currently studied as hydrotreating catalysts, as photocatalysts and as lubricants. Thus, having at hand a large-scale and facile preparation method we can systematically study the influence of slabs curvature and stacking on the activity and selectivity of HDS reaction. Furthermore, IF-
60 MoS_2 systems modified with promoters seem to be promising for

the preparation of thermally stable catalytic materials, as will be discussed elsewhere. In lubrication studies the novel materials will allow studying the influence of size and void-to wall thickness ratio on the tribological properties. Finally, such
65 systems appear to have potential in the photocatalytic production of hydrogen in the presence of sulfide ions.

Notes and references

a Institut de Recherches sur la Catalyse et l'Environnement de Lyon
70 *IRCELYON, UMR 5256, CNRS – Université Lyon 1, 2 av A. Einstein*
69626 Villeurbanne Cedex (France); Fax: 33 04 7244 5399; Tel: 33 04
72 44 5466; E-mail: pavel.afanasiev@ircelyon.univ-lyon1.fr
b IFP Energies nouvelles Rond-point de l'échangeur de Solaize BP3
69360 France
75

1 J.M. Lehn, *Science* 1985, **227**, 849.

2 P. G. Moses, B. Hinnemann, H. Topsoe, J. K. Nørskov, *J. Catal.* 2007, **248**, 188.

3 M. P. de la Rosa, S. Texier, G. Berhault, A. Camacho, M. J. Yacaman, A. Mehta, S. Fuentes, J. A. Montoya, F. Murrieta, R. R. Chianelli, *J. Catal.* 2004, **225**, 288.

4 a) T. F. Jaramillo, K. P. Jørgensen, J. Bonde, J. H. Nielsen, S. Horch, I. Chorkendorff, *Science* 2007, **317**, 100; b) V. W. Lau, A. F. Masters, A. M. Bond, T. Maschmeyer, *Chem. Eur. J.* 2012, **18**, 8230.

5 Y. Araki, K. Honna, H. Shimada, *J. Catal.* 2002, **207**, 361.

6 a) M. Chhowalla, G. A. Amaratunga, *Nature* 2000, **407**, 164; b) J. Tannous, F. Dassenoy, I. Lahouij, T. Le Mogne, B. Vacher, A. Bruhács, W. Tremel, *Tribol. Lett.* 2011, **41**, 55; c) I. Lahouij, B. Vacher, J. M. Martin, F. Dassenoy, *Wear* 2012, **296**, 558.

7 J. P. Lemmon, M. M. Lerner, *Chem. Mater.* 1994, **6**, 207.

8 M. S. Whittingham, *Science* 1976, **192**, 1126.

9 a) G. Eda, H. Yamaguchi, D. Voiry, T. Fujita, M. Chen, M. Chhowalla, *Nano Lett.* 2011, **11**, 5111; b) A. Splendiani, L. Sun, Y. Zhang, T. Li, J. Kim, C. Y. Chim, G. Galli, F. Wang, *Nano Lett.* 2010, **10**, 1271.

10 M. Naffakh, A. M. Díez-Pascual, C. Marco, G. J. Ellis, M. A. Gómez-Fatou *Prog. Polymer Sci.* 2013, **38**, 1163.

11 a) R.Tenne, L. Margulis, M. Genut, G. Hodes, *Nature* 1992, **360**, 444; b) D. J. Srolovitz, S. A. Safran, M. Homyonfer, R. Tenne, *Phys. Rev. Lett.* 1995, **74**, 1779; c) R. Tenne, *Nat. Nanotechnol.* 2006, **1**, 103; d) R. Rosentsveig, A. Margolin, A. Gorodnev, R. Popovitz-Biro, Y. Feldman, L. Rapoport, Y. Novema, G. Naveh, R. Tenne, *J. Mater. Chem.* 2009, **19**, 4368.

12 M. Nath, A. Govindaraj, C. N. R. Rao, *Adv. Mater.* 2001, **13**, 283.

13 C. M. Zelenski, P. K. Dorhout, *J. Am. Chem. Soc.* 1998, **120**, 743.

14 H. Topsøe, B. S. Clausen and F. E. Massoth, Hydrotreating Catalysis – Science and Technology, Springer, Berlin (1996).

15 P. A. Parilla, A. C. Dillon, K. M. Jones, G. Riker, D. L. Schulz, D. S. Ginley, M. J. Heben, *Nature* 1999, **397**, 114.

16 J. Etzkorn, A. H. Therese, F. Rocker, N. Zink, U. Kolb, W. Tremel, W. *Adv. Mater.* 2005, **17**, 2372; b) N. Zink, J. Pansiot, J. Kieffer, H.A. Therese, M. Panthofer, F. Rocker, U. Kolb, W. Tremel, *Chem. Mater.* 2007, **19**, 6391.

17 E. Devers, P. Afanasiev, B. Jouguet, M. Vrinat, *Catal. Lett.* 2002, **82**, 13.

18 D. Duphil, S. Bastide, C. Levy-Clèment, *J. Mater. Chem.* 2002, **12**, 2430.

19 a) N. A. Dhas, K. S. Suslick, *J. Amer. Chem. Soc.* 2005, **127**, 2368; b) I. Uzcanga, I. Bezverkhyy, P. Afanasiev, C. Scott, M. Vrinat, *Chem. Mater.* 2005, **17**, 3575.

20 L. X. Chang, H. B. Yang, J. X. Li, W. Y. Fu, Y. H. Du, K. Du, Q. Y. Yu, J. Xu, M. H. Li, *Nanotech*. 2006, **17**, 3827.

21 A. Nogueira, R. Znaiguia, D. Uzio, P. Afanasiev, G. Berhault, *Appl. Catal. A*. 2012, **429**, 92.

22 P. Afanasiev, I. Bezverkhyy, *Chem. Mater*. 2002, **14** 2826

23 L. Chang, H. Yang, W. Fu, J. Zhang, Q. Yu, H. Zhu, J. Chen, R. Wei, Y. Sui, X. Pang, G. Zou, *Mater. Res. Bull*. 2008, **43**, 2427.

24 P. K. Panigrahi, A. Pathak, *Mater. Res. Bull*. 2011, **46**, 2240.

25 K. Du, W. Fu, R. Wei, H. Yang, S. Liu, S. Yu, G. Zou, *Mater. Lett*. 2007, **61**, 4887.

26 Y. Xiong, Y. Xie, Zh. Li, X. Li, R. Zhang, *Chem. Phys. Lett*. 2003, **382**, 180.

27 B. O. Dabbousi, J. Rodriguez-Viejo, F. V. Mikulec, J. R. Heine, H. Mattoussi, R. Ober, K. F. Jensen, M. G. Bawendi, J. Phys. Chem. B 1997, **101,** 9463.

28 M. Ethayaraja, C. Ravikumar, D. Muthukumaran, K. Dutta, R. Bandyopadhyaya, *J. Phys. Chem. C* 2007, **111**, 3246.

29 P. Afanasiev, C. Geantet, I. Llorens, O. Proux, *J. Mater. Chem*. 2012, **22**, 9731.

30 S. J. Hibble, G. B. Wood, *J. Amer. Chem. Soc*. 2004, **126**, 959.

31 N. Uekawa, T. Matsumoto, T. Kojima, F. Shiba, K. Kakegawa, *Colloid Surf. A*, 2010, **361**, 132.

32 Y. Feldman, E. Wasserman, D. J. Srolovitz, R. Tenne, *Science* 1995, **267**, 222.

33 P. Afanasiev, *J. Catal*. 2010, **269**, 26.

34 Z. Vít, D. Gulková, L. Kaluža, M. Zdražil, *J. Catal*. 2005, **232**, 447.

35 E.J.M. Hensen, H.J.A. Brans, G.M.H.J. Lardinois, V.H.J. de Beer, J.A.R. van Veen and R.A. van Santen, *J. Catal*. 2000, **192**, 98.

36 A. Yella, M. Panthoefer, M. Kappl, W. Tremel, *Angew. Chem. Int. Ed.* 2010, **49**, 2575.

Graphical abstract for the paper

From core-shell MoS$_x$/ZnS to open fullerene-like MoS$_2$ nanoparticles.

Elodie Blanco[†], Denis Uzio[‡], Gilles Berhault[†], Pavel Afanasiev[†*]

[†]*Institut de recherches sur la catalyse et l'environnement de Lyon UMR5256, CNRS-Université de Lyon 1, 2 avenue Albert Einstein 69626 Villeurbanne cedex.* [‡]*IFP Energies nouvelles Rond-point de l'échangeur de Solaize BP3 69360 Solaize*
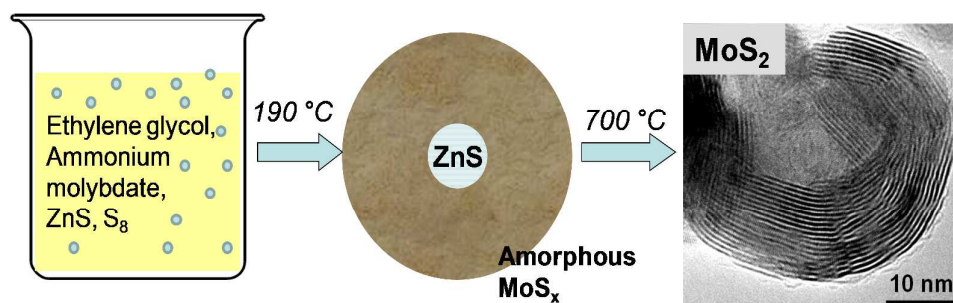
Text abstact for the contents page:

Open 20-50 nm size fullerene-like MoS$_2$ particles having controllable size and wall thickness were prepared with quantitative yield from the seed-grown core-shell materials MoS$_x$/ZnS (x~3-4).